Materials Advances

ROYAL SOCIETY OF CHEMISTRY

PAPER

View Article Online
View Journal | View Issue

Cite this: *Mater. Adv.*, 2024, 5, 8889

A cost-effective strategy to design and fabricate absorption dominant flexible multilayer laminates by rationally tailoring their layers†

Vaishnavi Khade,[a] Avanish Babu Thirumalasetty,[a] Yogesh Kumar Choukiker[b] and Madhuri Wuppulluri *[c]

Owing to the ever-increasing complexity of the electromagnetic environment, the market for electromagnetic interference (EMI) shielding is expanding at a rapid rate. Recently, there has been a focus on developing new methods that can be used to fine-tune and forecast the shielding qualities of buildings without using up all of the raw materials. Additionally, methods that are economical and need a short duration of time for optimization have been prioritized. The purpose of this article is to demonstrate an efficient and accurate method for predicting the EMI shielding effectiveness (EMI SE) of materials. This is accomplished by simulating the performance of composites that contain alternate layers of conducting and magnetic materials within a virtual waveguide measurement environment. Using CST Studio Suite software, the EMI shielding effectiveness of multilayered structures is simulated in the X-band range. The strategic arrangement of electromagnetic (EM) energy-trapping layers within impedance-matching layers in the multilayered structures is found to significantly contribute to the enhancement of absorption-dominated EMI shielding, as demonstrated through a simulation carried out by varying the order and number of the conducting and magnetic layers. Among the multilayered structures, the PC/PM/PC (PVDF-CNF/PVDF-MWCNTs/PVDF-CNF) systems showed the best shielding efficiency, with a value of 96.47 dB. Poly(vinylidene fluoride)-based composites comprising low-cost MWCNTs are used to construct the multilayered structures for testing purposes. After completing this research, we came up with the hypothesis that it is not required to use materials that have a high manufacturing cost and need laborious fabrication processes in order to create extremely effective shielding materials.

Received 23rd July 2024,
Accepted 27th September 2024

DOI: 10.1039/d4ma00741g

rsc.li/materials-advances

1. Introduction

EM radiation-based products and gadgets have grown increasingly essential in our daily lives ever since EM frequencies were first commercialized in the late 1800s. The amount of EM radiation surrounding us has unquestionably increased with the introduction of the internet of things (IoT) and advancements in technology, leaving us vulnerable to a complicated electromagnetic environment.[1–3] Furthermore, it is apparent in the current available literature that electromagnetic interferences have a disruptive effect on the optimal operation of sophisticated precision electronic devices utilized for advanced applications across diverse domains, including medicine, aerospace, and military sectors.[4–7] Moreover, numerous data indicate the detrimental effects of EM radiation on the overall health and welfare of humans and other living organisms.[8,9] Thus, there has been an increasing demand for the development of EMI shielding materials that are capable of efficiently mitigating electromagnetic waves. This demand arouses primarily as a result of the implementation of fifth-generation networks, which utilize higher-frequency electromagnetic radiation. Therefore, innovation in the development of technically improved EMI shielding materials and reinforcement of engineering strategies for shielding structures are urgently required.

Two basic mechanisms that are engaged in electromagnetic interference shielding are reflection and absorption. Therefore, electromagnetic interference shielding materials can be roughly categorized into two types: reflection-dominant shielding materials and absorption-dominant shielding materials. Despite the fact that metals, conductive polymers, and low-dimensional materials

[a] *Department of Physics, School of Advanced Sciences, Vellore Institute of Technology, Vellore, Tamil Nadu, India*
[b] *School of Electronics Engineering, Vellore Institute of Technolog, Vellore, Tamil Nadu, India*
[c] *Ceramic Composites Laboratory, Centre for Functional Materials, Vellore Institute of Technology, Vellore, Tamil Nadu, 632014, India. E-mail: madhuriw12@gmail.com*

† Electronic supplementary information (ESI) available. See DOI: https://doi.org/10.1039/d4ma00741g

such as reduced graphene oxide and MXenes can achieve high EMI SE, the inherent reflection of electromagnetic waves due to the conductivity of these materials can have adverse effects on the environment and electronic devices utilized in an enclosure for aerospace and military purposes.[10–13] The attainment of such material combinations can be accomplished through the appropriate integration of magnetic and conducting materials in order to facilitate impedance matching and consequently minimize the reflection of electromagnetic waves.[14] Additionally, it has been reported that the utilization of a multilayered configuration consisting of magnetic and conductive structures can effectively enhance the shielding capabilities of the composites. This is achieved by capitalizing on the phenomenon of multiple internal reflections that occur due to the impedance mismatch between the several layers with differing properties.[14,15]

The utilization of multilayered composites presents a compelling approach to mitigate reflection-based shielding by strategically arranging the conducting and magnetic layers in a certain order. Enormous research has been conducted to investigate the EMI SE of various arrangements of multilayered composite structures.[15–18] The method is further validated by recent review articles that explore the possibility of multilayered structures made of polymers for EMI shielding.[19–21] When using multilayer structures, the EMI shielding efficiency can be tuned by adjusting the concentration of the fillers, layer order, layer thickness, and layer number, as well as by choosing the conducting and magnetic fillers for each layer. A prevalent myth is that producing high-performance EMI shielding materials is too expensive, time-consuming, and labor-intensive for industrial integration because of the optimization step alone. Therefore, it is critical to innovate methods by implementing strategies that can yield good outcomes in a reasonable amount of time without wasting resources.

An intriguing and underexplored approach to predicting a material's EMI SE from its electrical conductivity and electromagnetic parameters is the use of simulation in the design of EMI shielding materials and then comparing and measuring the EMI shielding parameters as well. According to the literature, many studies have focused on fabricating and testing various microwave-absorbing and EMI shielding materials with different properties. However, very few have attempted to design EMI shielding materials using robust simulation tools and then validate the simulated results with the experimental results obtained after fabrication. For X-band applications, Liu *et al.* and Kashi *et al.* utilized CST Studio Suite in 2020 to investigate and optimize the EMI shielding characteristics of textiles modified with Ag nanowires and poly- (butylene adipate-*co*-terephthalate) and poly-lactide nanocomposites incorporating graphene, respectively.[22] Phan *et al.* also investigated the use of the high frequency structure simulator (HFSS) to conduct simulation-based EMI shielding investigations on transparent shielding applications involving multilayered salt-water in planar acrylic and glass within the frequency range of 7.5–8.5 GHz.[23] Subsequently in 2022, Hu *et al.* conducted simulations within the 1.0–1.5 GHz frequency range on the optimized textile model in order to optimize a multitude of parameters for shielding applications based on textiles.[24]

This study details a novel systematic simulation analysis of multilayered composites made of conducting and magnetic filler-reinforced polymers along with experimental evidence for the purpose of mitigating electromagnetic radiation. $Co_{0.9}$-$Ni_{0.1}Fe_2O_4$ (CNF) is used as a magnetic filler, multiwalled carbon nanotubes (MWCNTs) are used as the conductive filler and poly(vinylidene fluoride) (PVDF) is the selected polymer matrix because of its exceptional mechanical qualities. The multilayer structures are created by stacking the single-layers that are produced using the doctor blade process and then hot-pressing these individual layers. This paper further dives into measuring EMI shielding efficiency and understanding the EMI shielding mechanism of multilayer structures with different layered configurations and numbers of layers by modelling the electromagnetic characteristics of the individual layers using CST Studio Suite software along with visualization of electric and magnetic field propagations through individual layers as well as multilayer structures. This work primarily focused on three arrangements: (1) PC/PM (PVDF-CNF/PVDF-MWCNTs), (2) PC/PM/PC (PVDF-CNF/PVDF-MWCNTs/PVDF-CNF), and (3) PM/PC/PM (PVDF-MWCNTs/PVDF-CNF/PVDF- MWCNTs). We take a close look at the underlying mechanisms that increase the shielding efficiency of multilayer structures, highlighting the importance of choosing the correct sequence and number of layers. In conclusion, this paper mainly delves into the function of simulation in engineering, design, and prediction of laminated structures, as well as their capacity to protect against electromagnetic radiation, with enough supporting experimental evidence.

2. Materials and methods

2.1. Simulation

All of the EMI shielding structures that are addressed in this study have been constructed and simulated in the X-band region by utilizing the finite element method using CST Studio Suite software. This involves developing a virtual EMI shielding measurement setup (see ESI,† Section S1 for details of the virtual wave guide environment). This is accomplished by designing a rectangular waveguide and placing the material under test (MUT) between port-1 and port-2 of the waveguide. The multilayer structures are constructed by assigning the electromagnetic parameters and electrical conductivity to individual layers, which will contribute to the total EMI shielding efficiency (SE_T) of multilayer structures.

The simulated structures are shown in Fig. 1(a)–(c). Shielding effectiveness is evaluated based on absorption (SE_A), reflection (SE_R), and total shielding (SE_T) using the reflection (S_{11}, S_{22}) and transmission scattering characteristics (S_{12}, S_{21}) derived from the following equations:

$$SE_A\,(dB) = -10\log\left(\frac{{S_{21}}^2}{1-{S_{11}}^2}\right) \quad (1)$$

$$SE_R\,(dB) = -10\log\left(1-{S_{11}}^2\right) = -10\log\left(1-{S_{22}}^2\right) \quad (2)$$

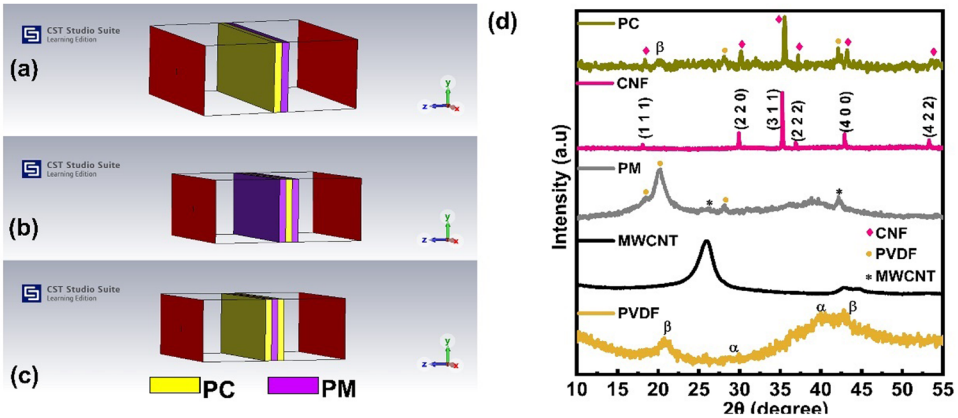

Fig. 1 (a)–(c) Model of simulated multilayer structures in CST Studio Suite software and (d) XRD pattern for pure PVDF, PM, and PC layers.

$$SE_T = SE_A + SE_R + SE \quad (3)$$

where SE_M represents the shielding caused by multiple internal reflections and can be disregarded if SE_A exceeds 10 dB.[25]

2.2. Fabrication of multilayer structures

The multilayer structures consisting of conductive MWCNTs (AdNano Technologies Pvt. Ltd., 99% purity) and magnetic CNF layers are prepared through a solvent casting and hot-pressing method. The synthesis of CNF is outlined in Section S2 (ESI†). In order to create separate conducting and magnetic layers, 1 g of PVDF powder is dissolved in 5 ml of *N*,*N*-dimethylformamide (DMF). 15 wt% MWCNTs is added to the fully dissolved uniform PVDF-DMF mixture and stirred overnight using a magnetic stirrer set at a speed of 300 rpm. The solution is subjected to sonication for a duration of 30 minutes using a bath sonicator maintained at room temperature. Ultimately, using the doctor blade technique the film is produced and maintained at ambient temperature for 24 h in order to achieve a consistent and even PC layer. A similar method is employed to manufacture the PM magnetic layer. The CNF layer is fabricated with 15 wt% of CNF.

The multilayered structures PM/PC, PM/PC/PM, and PC/PM/PC are created by stacking alternating layers of PM and PC (see Fig. 1(a)–(c)). The composites are subsequently exposed to hot-pressing at a temperature of 220 °C for a duration of 15 minutes, with minimal applied pressure. The PM/PC is a combination of a conducting and magnetic layer. PM/PC/PM and PC/PM/PC composites consist of a conducting layer sandwiched between two magnetic layers, and *vice versa*, respectively. The PM/PC, PM/PC/PM, and PC/PM/PC composites consist of a sequential arrangement of conducting and magnetic layers. There is a total of 2- and 3-layers, each with a uniform thickness of 3.8 mm (see ESI,† Fig. S1(a) for the schematic of preparation of multilayer structures).

2.3. Characterization

The degree of crystallinity and identification of phases in CNF and individual layers of multilayer structures are examined using X-ray diffraction (XRD) (BRUKER D8 advanced X-ray diffractometer) with Cu K_α radiation (λ = 1.5406 Å). The scanning range is set from $2\theta = 10^\circ$ to 80°. The individual composite layers are analyzed for their microstructure using a field emission scanning electron microscope (FESEM) (Thermo Fisher Scientific FEI Quanta 250 FEG). The electromagnetic properties of the individual layers in the X-band range are also determined using the waveguide approach. The conductivity of the individual layers of multilayer structures is determined based on the complex permittivity of the composites. The SE_T of the individual layers as well as multilayer structures in the X-band region is determined by analyzing the reflection and transmission scattering parameters. These parameters are assessed using a vector network analyzer (VNA) (Anritsu) through the transmission-line method.

3. Results and discussion

3.1. Characterization of individual PM and PC layers

Before moving to the characterization of individual layers, the characteristics of synthesized CNF are presented and discussed elsewhere.[26] The XRD patterns of individual PM and PC layers are graphically represented in Fig. 1(d). Confirmation of the cubic structure of CNF is provided by the data presented in Fig. 1(d), which is indexed at $2\theta = 18^\circ$ (1 1 1), 29.9° (2 2 0), 36.9° (3 1 1), 42.9° (2 2 2), 53.3° (4 2 2), 56.8° (5 1 1), and 62.4° (4 4 0). Upon examination of the X-ray diffraction pattern for PM, it is evident that the diffraction peaks that correspond to the (3 1 1) crystal planes of CNF and the β-phase peak of PVDF are present. In a similar manner, it is observed for the PC film. No secondary peaks are noticed, confirming the formation of the PM and PC composite films.

The morphology studies of the individual PC and PM layer are shown in Fig. 2(a) and (b). Fig. 2(a) depicts the distribution of CNF throughout the PVDF matrix, and the morphology reveals that PVDF granules have been created in a clear and distinct manner. It has also been observed that the PM layer has a higher degree of porosity in comparison to the rigid CNF discussed in the article.[26] Therefore, with reference to EMI shielding, the porous layer of the PC contributes to the

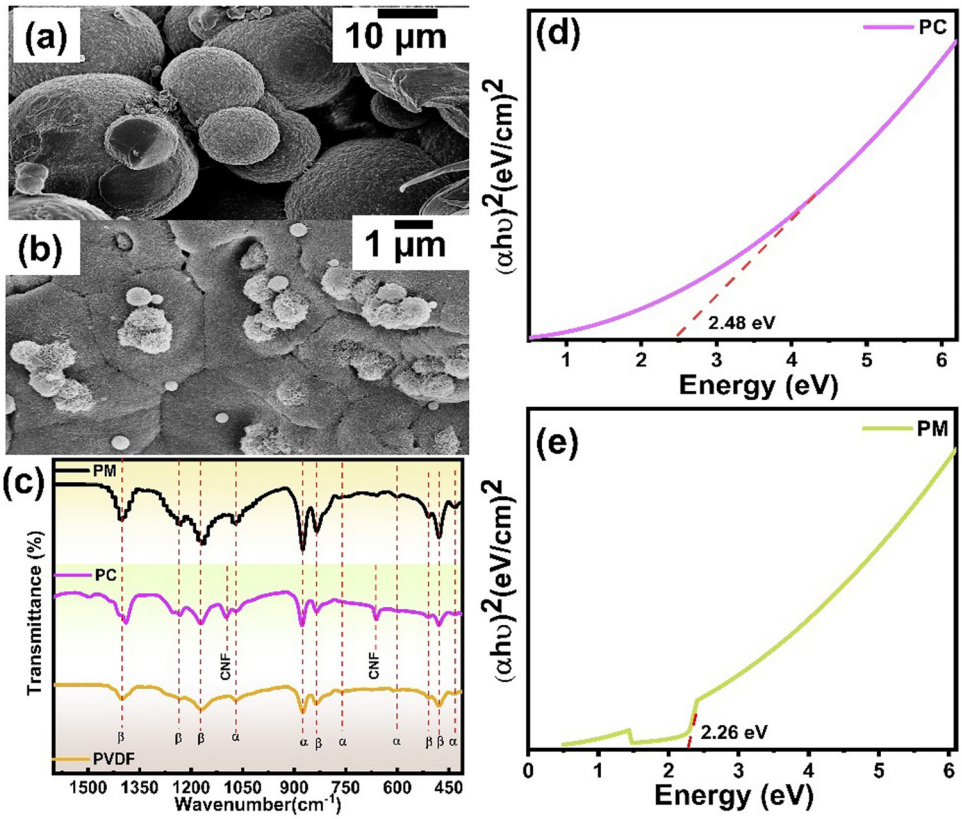

Fig. 2 (a) and (b) SEM images for PC and PM layers, respectively, (c) FT-IR studies of pure PVDF, PM, and PC layers and (d) and (e) band gap studies for PC and PM layers.

enhancement of the effectiveness of absorption shielding. An SEM image of the PM layer (see Fig. 2(b)) clearly demonstrates the presence of MWCNTs, which indicates that they are distributed uniformly throughout the PVDF matrix. The FTIR absorption spectra of a pure PVDF film, the individual PC and PM layer are shown in Fig. 2(c). In the FTIR spectrum of PVDF, absorption bands are observed at 614, and 763, and 795 cm^{-1} (as shown in Fig. 2(c)). These bands are associated with the mixed CF_2 bending, and C–C–C skeletal vibration, respectively, for the α-phase.[27] Furthermore, a distinct low- intensity band at 1275 cm^{-1} is noted, indicating the existence of the β-phase. It may be deduced that the pure PVDF material does not contain the γ-phase because there is no band at 1234 cm^{-1}. So, it's reasonable to assume that the α-phase makes up the majority of the pure PVDF film, while the β-phase is indicated by bands at 1275 cm^{-1}, 841 cm^{-1}, and 510 cm^{-1}. Fig. 2(c) shows the FTIR spectrum of the PC and PM layer. The spectra show a pattern similar to that of PVDF, as previously noted. The PC layer additionally shows a band at a frequency of 560 cm^{-1}, which corresponds to the stretching vibrations of the metal–oxide groups that are situated in the tetrahedral sites of ferrite.[28] The Fe–Co bond is responsible for the band found at 1155 cm^{-1}.[29]

The band gap energy is the amount of energy that is required to excite an electron from the valence band to the conduction band. The calculation of the band gap energy with precision is very necessary in order to accurately predict the electromagnetic absorption characteristics of the multilayer structure, it is essential to ensure that the band gap energy of individual layers of the multilayer structure is calculated. The E_g is obtained by analyzing the tangent that is extrapolated to the *X*-axis of the 'Tauc' plots (see Fig. 2(e) and (f)) and the formula used to find the band gap is discussed in Section S3 (ESI†).[30] The E_g values for PC and PM layers are 2.48 eV and 2.26 eV, respectively. It has been demonstrated that the band gap decreases with the addition of CNF and MWCNT when compared to pure PVDF (see Fig. S2(a), ESI†). Thus, it may enhance EMI shielding efficiency by forming a conductive network.

Electrical conductivity (σ) is an essential factor that plays a significant role in determining the EMI shielding ability of a material. This is because σ is directly related to both SE_R and SE_A.[21,31] In addition, it is a well-established fact that an increase in electrical conductivity leads to an increase in reflection. As a result, the amount of conductive filler in the matrix and the arrangement of the system that involves the conducting layers may be adjusted to achieve the desired level of shielding. Fig. 3(a) shows the electrical conductivity of the individual PM and PC layers. In the case of the PM and PC layers, they exhibited an electrical conductivity of 3.5 and 2.79 S m^{-1}, respectively. A minor increase in conductivity is shown for the multilayer structures as the number of layers

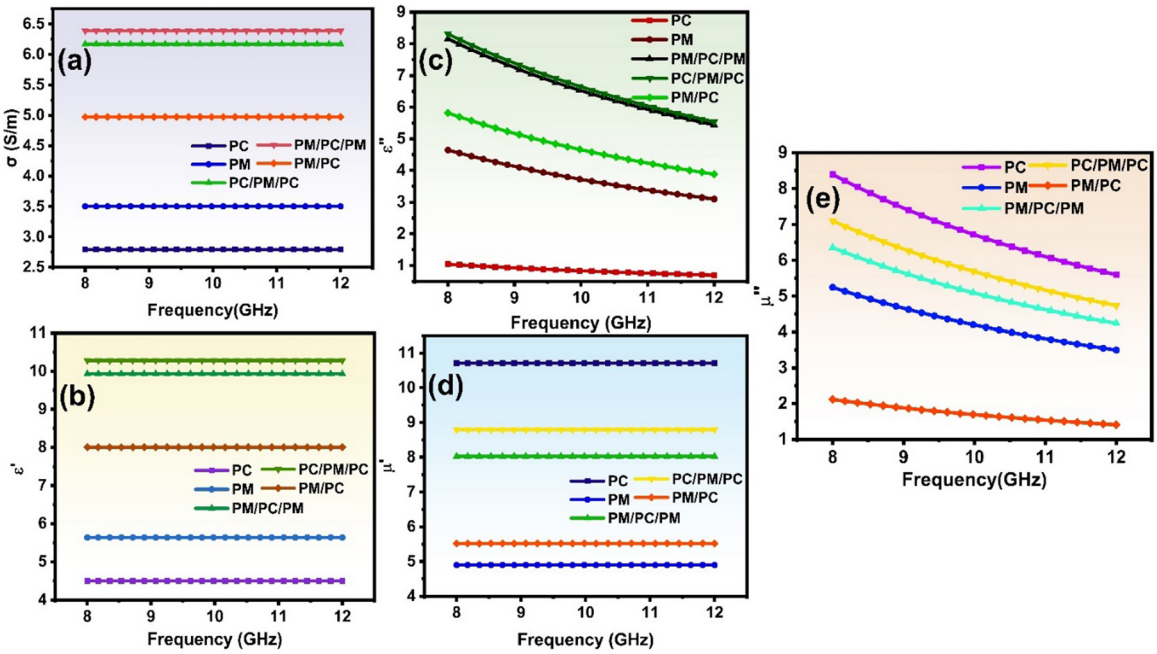

Fig. 3 (a) Electrical conductivity *versus* frequency for individual and multilayer structures and (b)–(e) electromagnetic characteristics for individual and multilayer structures.

increases. In addition, it is important to understand that the sequence in which the layers are arranged is a significant factor in determining the conductivity of the composites. Due to the absence of a conductive upper and lower layer, the conductivity of the PC/PM/PC structure is seen to decrease by a significant amount. This is in accordance with the findings of Guo *et al.*[25]

The electromagnetic properties of a shielding material have a significant impact on the EMI shielding performance. Complex permittivity ($\varepsilon_r = \varepsilon' - j\varepsilon''$) and complex permeability ($\mu_r = \mu' - j\mu''$) are the parameters that characterize the electromagnetic (EM) properties of a material, where the imaginary parts of permittivity and permeability correlate with the EM energy losses (ε'' and μ''), and the real component of permittivity and permeability (ε' and μ') is assigned to the electromagnetic energy retention potential when it comes to electromagnetic energy. Fig. 3(b) and (c) illustrates the dielectric constant and loss of the PM and PC layer in the 8–12 GHz frequency range. In comparison to the PC, the PM layer has the highest permittivity. This can be due to the high electrical conductivity of the MWCNTs present in the matrix, as well as the added Maxwell–Wagner–Sillars (MWS) polarization. Due to the discrepancy in their electrical conductivity, the free charge carriers will be trapped at the filler–matrix interfaces in heterogeneous systems. This will result in the formation of MWS polarization, which is a result of the contribution of both the migrating and the hopping electrons.[32,33] It can be observed from Fig. 3(b) that the PC layer has the lowest permittivity, in accordance with the lowest conductivity of the layer. In the case of the multilayer structures, the PC/PM/PC exhibits a higher permittivity than PM/PC/PM and PM/PC, which agrees with the trend in electrical conductivity of the multilayer structures. The analysis of the dielectric loss (see Fig. 3(c)) revealed that the PM layer presents more dielectric loss than the PC layer, which might be attributed to the conduction losses associated with percolative composite systems. In the case of PM/PC (see Fig. 3(c)), the high dielectric loss stems from the ohmic losses contributed by the well-connected conductive network formed by MWCNTs and the polarization losses arising from the increased interfaces in the composite.[33] The PC layer exhibited a dielectric loss of 0.725 (see Fig. 3(c)). The dielectric loss of the multilayer structures PC/PM/PC and PM/PC/PM followed the same trend as observed in the case of real permittivity (see Fig. 3(c)). The curve in Fig. 3(d) and (e) depicts the magnetic permeability and losses of the PM, PC/PM, PM/PC/PM and PC/PM/PC structures as a function of frequency. It is possible to ascribe the magnetic permeability of ferrites to the domain wall motion that is common in low-frequency regions as well as the gyromagnetic spin rotation that is predominant in high-frequency regions.[34] The μ' values of all the structures followed a steady a pattern with an increase in frequency. This trend is in line with the observations made on ferrite-based composites that have been documented in the literature.[35,36] As can be seen in Fig. 3(d) and (e), the magnetic permeability and loss of the multilayer structures are lower than those of the individual magnetic PC layer. One possible explanation for this is that the inclusion of nonmagnetic MWCNTs results in a decrease in the magnetic characteristics of the material. Over the X-band, the electromagnetic properties of each of the composites are tabulated in Table 1. It is clear that the conducting PM layer and the magnetic PC layer each provide a unique contribution to the improved shielding behaviour of the multilayered structures. This is demonstrated by the high

Table 1 Electromagnetic parameters for individual and multilayer structures

Composite	ε'	ε''	μ'	μ''	σ (S m^{-1})
PM	5.64	3.34	—	—	3.50
PC	4.49	0.73	10.71	5.86	2.79
PM/PC	8.0	4.06	5.52	1.48	4.97
PM/PC/PM	9.93	5.8	8.02	4.44	6.39
PC/PM/PC	10.28	5.69	8.79	4.96	6.17

dielectric loss of the PM layer and the superior magnetic characteristics of the PM layer.

3.2. Simulation

The capability of a material to provide protection against electromagnetic radiation is referred to as the EMI shielding effectiveness. Three mechanisms—reflection, absorption, and multiple internal reflections—are responsible for determining the overall EMI shielding performance of any material. It is therefore possible to express the entire shielding efficiency as the sum of SE_R, SE_A, and SE_M, as shown in eqn (5). SE_R is highly dependent on the electrical conductivity of the shielding material since the shielding that is induced by reflection occurs as a result of the interaction between the charge carriers and the electromagnetic field. It is possible to express it in decibels by using the following equation:

$$SE_R = -10\log\left(\frac{\sigma}{32\pi f \varepsilon_0 \mu}\right) \quad (4)$$

Similarly, shielding due to absorption can be given as

$$SE_A = -8.7d\sqrt{f\pi\sigma\mu} \quad (5)$$

where σ is the total conductivity, μ is the relative permeability, ε is the relative permittivity, f is the frequency, and d is the thickness of the material. To be suitable for commercial use, a material's overall EMI shielding efficiency must be higher than 20 dB, which translates to a 99% attenuation of electromagnetic waves.

3.2.1. Simulated EMI shielding properties of multilayered structures. It is evident from eqn (5) that the electrical conductivity of a material, in addition to the relative permeability of the material, acts as a defining factor for the absorption of the material. In light of this, a suitable shielding material should be the combination of the attributes that are required by eqn (5) and (6). Providing specific input data, such as the electrical conductivity and electromagnetic properties of the materials involved, is essential in order to simulate the EMI shielding efficiency of any structure. Therefore, the input parameters of individual PM and PC layers that are utilized for simulations are investigated and tabulated in Table 1. Section 3.2.2 has a comprehensive examination of these factors. These values are used to simulate the multilayer structures at the microwave frequencies. Using CST Studio Suite software, reflection loss (RL) characteristics are predicted for the multilayer structures in the 8–12 GHz range.

The simulated RL curves of the individual layers PM and PC and multilayer structures PM/PC, PM/PC/PM, and PC/PM/PC

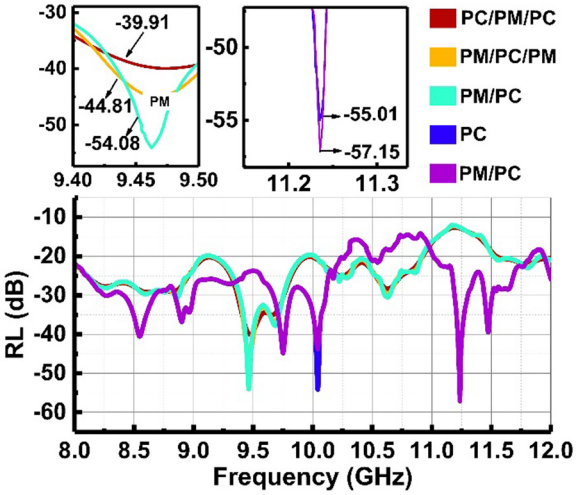

Fig. 4 RL simulated for individual and multilayer structures.

are presented in Fig. 4. The predicted RL of the composites from the simulation is in the order of PC/PM/PC > PM/PC/PM > PM/PC > PC > PM. Fig. 5(a)–(d) and animated videos in Supporting information V1(a)–(d) (ESI†) show the electric field and magnetic field propagation in the waveguide with PC/PM/PC and without the material (see the animated videos in Supporting information V2(a)–(d), ESI†). For PM/PC, and PM/PC/PM the electric and magnetic field propagation through the material in the waveguide is presented in Fig. S2(b) (ESI†). It is noteworthy to observe that the RL of PM/PC, PM/PC/PM, and PC/PM/PC multilayer structures is superior to that of the individual PM and PC layers. Furthermore, the PM/PC/PM structure displayed a RL that is greater than that of the PM/PC and PC/PM/PC, while having a conductivity that is significantly higher. From the results it is understood that when it comes to multilayer structures, the sequence in which the layers are arranged is a significant factor. Additional mechanisms that are involved are the conduction losses that occur from the PM, the polarization losses that occur from the PM, the magnetic losses, and the many internal reflections that occur at the interface between the PM and PC.[33]

3.3. Testing the EMI shielding properties of multi-layered structures

Fig. 6(a) illustrates the frequency response curves of the composites, with respect to reflection loss (RL) characteristics for PM, PC, PM/PC/PM, and PC/PM/PC. It is evident from the illustration that the maximum difference between the simulated and measured RL values does not exceed 5 dB. The reflection losses are found to rise with the number of layers and the arrangement of individual layers, which has an effect on the absorption properties of multilayer structures. When compared to other structures, the PC/PM/PC exhibits a larger reflection loss of −34.49 dB (see Table 2), which indicates that 99.99% of electromagnetic waves are absorbed, hence increasing the number of electromagnetic waves that are absorbed. This topic will be covered in greater depth in subsequent Section 3.3.1.

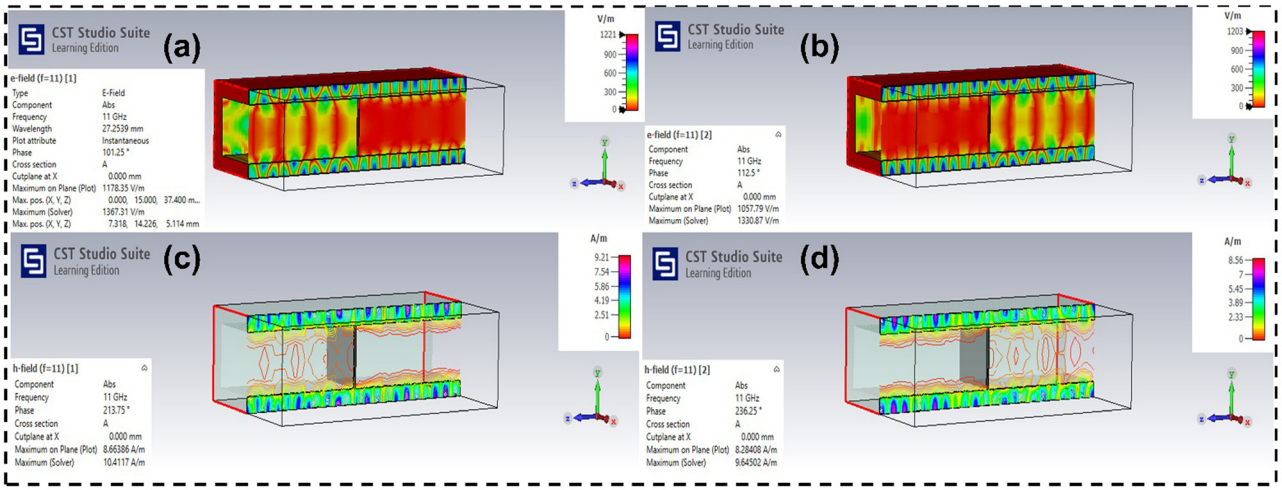

Fig. 5 (a) and (b) Electric field propagation for PC/PM/PC and (c) and (d) magnetic field propagation for PC/PM/PC.

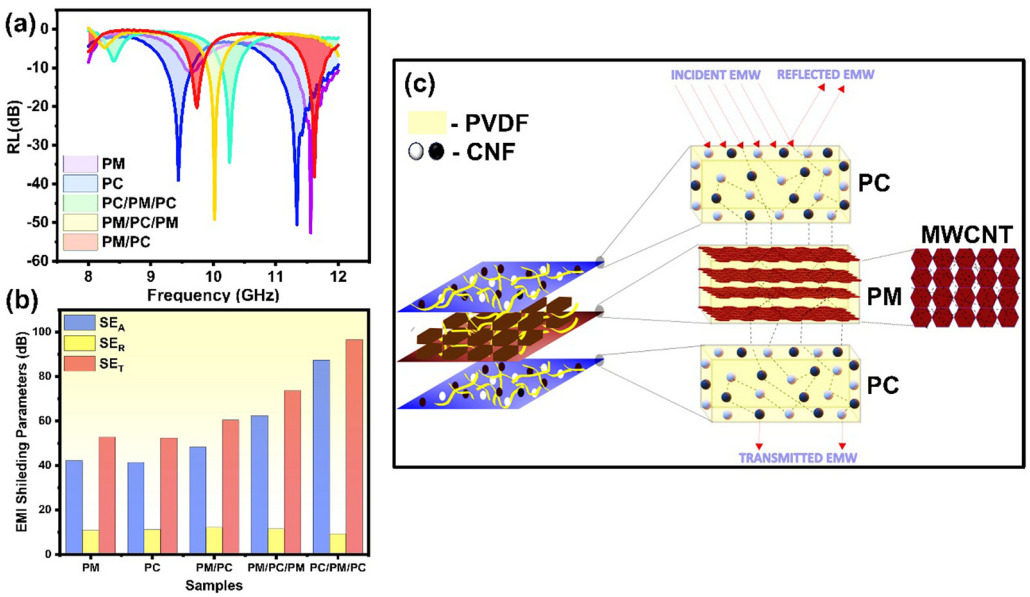

Fig. 6 (a) Experimental RL for individual and multilayer structures, (b) EMI shielding parameters for individual and multilayer structures, and (c) EMI shielding mechanism for individual and multilayer structures PC/PM/PC.

The SE_A, SE_R, and SE_T as a function of frequency are displayed in Fig. 6(b) for PM, PC, PM/PC, PM/PC/PM, and PC/PM/PC structures. The measurements demonstrate that PC/PM/PC has the highest SE_T value with a large increase in SE_A without a corresponding rise in SE_R compared to other developed structures (see Table 2). Furthermore, the SE_T of the manufactured structures clearly demonstrates an impact of the arrangement of the conducting and magnetic layers. The experimental data indicate that the arrangement of layers is a crucial factor in regulating the reflection-based shielding and electromagnetic energy trapping in the multilayer structures. This finding aligns with the outcomes derived from the simulation. The reason behind the larger SE_T value of PC/PM/PC structures than other structures is discussed in Sections 3.3.2. and 3.3.3.

Table 2 EMI shielding efficiency and parameters for individual and multilayer structures

Sample	RL simulated (dB)	RL (dB)	SE_A (dB)	SE_R (dB)	SE_T (dB)
PM	−52.66	−57.15	42.14	10.66	52.79
PC	−50.50	−53.72	41.33	11.03	52.36
PM/PC	−49.18	−54.08	48.28	12.04	60.32
PM/PC/PM	−38.2	−44.81	62.21	11.35	73.55
PC/PM/PC	−34.49	−39.91	87.37	9.10	96.47

3.3.1. Mechanism of EMI shielding. Fig. 6(c) illustrates the mechanism behind attenuating electromagnetic radiation in multilayered structures. It is the separate contributions of the conducting PM layer and the magnetic PC layer that are responsible for the attenuation of electromagnetic energy in the

multilayer structure. Additionally, the specific layered arrangement is responsible for trapping of the EM energy. In the PC/PM/PC configuration, whereby conductive reflective layers are placed between impedance-matching layers, the incident electromagnetic wave will experience low primary reflection in contrast to the PM/PC/PM structure, whereby the reflections of electromagnetic waves will be more pronounced at the interface between the main electromagnetic wave and the material. Additionally, the incident wave will experience absorption at the magnetic PC layer as a result of the magneto-dielectric properties of PC. Polarization losses and magnetic losses contribute to the attenuation at the magnetic PC layer. At the PC layer, there are two types of polarization losses that can occur: dipolar polarization loss, which is caused by the magnetic filler, and interfacial polarization loss, which is caused by the interfaces between the filler and matrix. First discussing the dipole polarization loss, the polarization relaxation process is a contributing factor to it. So, to estimate this, Debye's theory is employed which gives a correlation between ε' and ε''[37] (see eqn (6)).

$$\left(\varepsilon' - \frac{\varepsilon_s - \varepsilon_\infty}{2}\right)^2 + \left(\varepsilon'' - \frac{\sigma}{\omega\varepsilon_o}\right)^2 = \left(\frac{\varepsilon_s - \varepsilon_\infty}{2}\right)^2 \quad (6)$$

where ω is the angular frequency, σ is the conductivity, ε_0 is the permittivity in vacuum, ε_s is the permittivity in the electrostatic field, and ε_∞ is the permittivity at the high-frequency limit, respectively. Fig. S3 (ESI†) depicts the Cole–Cole plot for the PC layer, which explains the relaxation nature in the PC layer. The observed semicircle of the plot is indicative of the Debye relaxation polarization. Since there are many relaxations, the semicircle takes on an arc shape and the radius of the circle suggests high degree of polarization. Furthermore, the length of the sloped straight line is a good indicator of the significant conduction loss. The conduction loss of the PC to EMWs is proportional to the length of the inclined straight line.[38] Generally speaking, the conduction loss of the PC is shown by an inclined straight tail in the Cole–Cole curve.[39] Conductivity loss is proportional to the slope of the inclined straight tail, and it increases as the slope increases.[40] When electromagnetic radiation is directed towards the magnetic PC layer, it will lead to the formation of induced dipole moments in the CNF molecules. When the dipoles come into contact with the incident electromagnetic radiation, a damping effect occurs, leading to dipolar losses and a reduction in the intensity of the electromagnetic radiation. The occurrence of Maxwell–Wagner–Sillars (MWS) polarization, also known as interfacial polarization, is primarily attributed to the buildup of charge at the interfaces. This phenomenon is particularly prominent in heterostructures that contain a significant number of heterojunctions.[33] At these junctions, the electromagnetic waves will experience attenuation as a result of interfacial relaxation losses. In addition, the presence of filler-matrix heterojunctions in the magnetic layer will result in numerous internal reflections and dispersion of electromagnetic waves, ultimately causing a decrease in electromagnetic energy. In addition to polarization losses, electromagnetic waves will also experience attenuation as a result of magnetic losses.[41] Magnetic losses in composites containing ferrite are primarily attributed to three factors: eddy current, hysteresis, and resonance.[42] The occurrence of both eddy current loss and hysteresis loss results in the transformation of electromagnetic energy into thermal energy, which then disperses throughout the material. Subsequently, the electromagnetic radiation that has experienced primary attenuation at the magnetic layer will be directed towards the conducting layer. In the PM layer, the electromagnetic wave will experience attenuation as a result of ohmic loss caused by the presence of MWCNTs, as well as interfacial polarization loss arising from the interfaces between MWCNTs and PVDF. In the case of highly conductive MWCNTs, the presence of migrating electrons leads to a considerable reduction in electromagnetic energy at the PM layer. The MWCNTs-PVDF junctions inside the PM layer will also result in heterojunctions exhibiting varying conductivity, leading to the occurrence of MWS polarization and subsequent relaxation in response to electromagnetic radiation. Moreover, electromagnetic waves will also experience many internal reflections and scattering at the interfaces between the filler and matrix, resulting in the absorption of electromagnetic radiation. Electromagnetic waves will experience a degree of reflection at the PM layer as a result of the layer's conductive properties. The weak secondary electromagnetic waves will experience attenuation at the PC layer and will finally emerge from the shielding structure as secondary reflections. As shown in Fig. 6(c), electromagnetic radiations that successfully traverse the second layer within the multilayer structure will experience further attenuation at the PC layer, which serves as the third layer.

In the cases of PM/PC and PM/PC/PM structures, electromagnetic radiation will be incident on the conducting PM layer, which will then reflect the electromagnetic waves back to the source. It is expected that the electromagnetic waves that are transmitted from the PM layer in the case of the PM/PC structure will be absorbed at the PC layer due to impedance matching, whereas for PM/PC/PM these are caught between the conducting PM layer and the magnetic PC layer (see Fig. 6(c)). With the distinct contributions of the conducting and magnetic layers, as well as the various back-and-forth reflections of electromagnetic waves that occur within the energy-trapping layers, the electromagnetic energy will be greatly reduced.

3.3.2. Influence of the order of layers in multilayer structures. Let us take into consideration the shielding structures of the PM/PC/PM and PC/PM/PC. When it comes to the PM/PC/PM composite, the conducting layers PM are located in the first and final layers. The inclusion of highly percolative conductive layers in the composites plays a crucial role in enhancing conduction losses. Since both SE_A and SE_R are directly related to electrical conductivity, electromagnetic energy absorption and reflection take place when electromagnetic waves come into contact. Upon entering the PM/PC/PM structure, they undergo the initial reflection followed by the subsequent encounter at the magnetic layer. This layer's permeability will decrease SE_R and increase SE_A (see Fig. 6(b)). The absorption

capabilities of the PC layer may be enhanced by addressing the magnetic losses, namely, the hysteresis loss and eddy current loss.[14] Moreover, it is important to note that there will be numerous internal reflections taking place at the interfaces between the layers and the filler-matrix interfaces. Ultimately, the waves will impinge against the last boundary of the composite material, which concurrently serves as a conductive layer. The conductive layer's reflecting properties will be advantageous in this case, as the electromagnetic waves that encounter this layer will be reflected back to the material, resulting in more dissipation of electromagnetic energy. In this specific configuration, the primary factor contributing to electromagnetic energy attenuation is reflection, followed by absorption.[15] This specific configuration of layers can be referred to as ''senticing layers,'' which reduce the EM energy by reciprocal reflections at the conductive layers PM, resulting in the subsequent absorption of EM energy.

For the PC/PM/PC composite, the impedance matching provided by the first magnetic layer PC (see Fig. S4(a) (ESI†) for impedance matching degree of PC and PM) makes it possible for electromagnetic waves to penetrate the sample in an effective manner; hence, the reflection is minimum, thus justifying the low SE_R value of PC/PM/PC (see Fig. 6(b)). Due to magnetic losses associated with the magnetic layer, the conduction losses associated with the conductive layer, and the dielectric losses, the electromagnetic wave that is introduced will be reduced in intensity. On the other hand, the waves that travel through the second conductive layer will come to interact with an impedance matching-magnetic layer. Despite experiencing attenuation because of magnetic and polarization losses, in contrast to the PM/PC/PM structure, some electromagnetic waves that remain unattenuated will traverse the last boundary of the composite material. The effectiveness of EM wave trapping is limited due to the arrangement of impedance-matching layers on both the front and back. Nevertheless, the utilization of PC/PM/PC ordering offers benefits in terms of reducing SE_R. To enhance the shielding efficiency of the multilayer structure, it is advisable to carefully choose a highly conductive layer as the intermediate layer. The results obtained from studying the EMI shielding mechanism of the PC/PM/PC and PM/PC/PM structures suggest that the specific arrangement of the layers significantly improves the efficiency of shielding in multilayer structures. Further, to justify the obtained SE_T values for multilayer structures attenuation constant studies are carried out, which agrees well with SE_T values (see Fig. S4(b), ESI†).

3.3.3. Influence of the number of layers in multilayer structures. In order to study the effect of the number of layers in the multilayer structures, a comparison is made between the EMI shielding properties of the 2-layer (PM/PC) and 3-layer (PM/PC/PM and PC/PM/PC) structures. From the tested RL values of the structures with a constant thickness of 3.8 mm in the X-band region, depicted in Fig. 6(a), it is clear that the number of layers has a significant impact on the total shielding efficiency of the material. In the case of the 2-layer (PM/PC) structure when the EM wave encounters this structure, due to PC being the first layer to interact, due to impedance matching the EM wave penetrates and strikes the PM layer. At PM, due its high electrical conductivity it is reflected back to the first layer and this process goes on. Some unattenuated waves transmit from the second layer and come out. As we increase the number of layers, the absorption of EM radiation increases *via* increased multiple internal reflections.

4. Conclusion

This study focuses on a simulation-based methodology to fabricate multilayered structures that exhibit enhanced electromagnetic interference shielding performance. The study primarily involves simulating several layered structures with varying layer patterns and number of layers. It is observed that the efficiency of shielding in multilayered structures is directly influenced by the order and number of layers. Moreover, thorough examinations of the impact of layer order on SE have shown that the careful selection of an appropriate configuration of the conducting and magnetic layers is crucial in improving the shielding effectiveness of the multilayered structures. The simulation of multilayered structures demonstrates that the strategic placement of the impedance matching layers in PC/PM/PC structures significantly improves absorption-dominated shielding by enhancing numerous internal reflections. PC/PM/PC structures provide a superior shielding efficiency of 96.47 dB compared to PM/PC/PM structures, with about 99% of the EM radiation attenuation being attributed to absorption. The EMI SE tests conducted on 2-layer (PM/PC) and 3-layer (PM/PC/PM and PC/PM/PC) structures show that the shielding characteristics of all the developed composites closely match the simulation results. This suggests that electromagnetic modelling is a highly effective method for forecasting the shielding characteristics of different structures with low requirements, and it can be used for all frequency ranges within the microwave spectrum. The findings of this study indicate that it is feasible to build microwave-absorbing structures with great efficiency by strategically arranging layers in magnetic-conducting topologies, without the need for expensive raw materials. Moreover, this study highlights a significant concept that electromagnetic simulation has great potential to design and optimize the EMI shielding characteristics of materials before the manufacturing stage of the systems. This enables the development of shielding structures with exceptional properties without depleting resources and capital.

Author contributions

V. K.: synthesis, data collection, draft preparation; A. B.: synthesis, data collection, draft preparation; Y. C.: EMI data curation and discussions; W. M.: conceptualization, methodology, final drafting and supervising the project.

Data availability

Data will be made available on request.

Conflicts of interest

The authors declare no competing financial interest.

Acknowledgements

The authors would like to thank the SAS, VIT University, for XRD, UV-vis, FTIR facilities. Thanks to Hyderabad Central University for FESEM facilities.

References

1 J. C. Shu, W. Q. Cao and M. S. Cao, Diverse Metal–Organic Framework Architectures for Electromagnetic Absorbers and Shielding, *Adv. Funct. Mater.*, 2021, **31**(23), 1–20, DOI: 10.1002/adfm.202100470.

2 Y. Wan, P. Xiong, J. Liu, F. Feng, X. Xun, F. M. Gama, Q. Zhang, F. Yao, Z. Yang, H. Luo and Y. Xu, Ultrathin, Strong, and Highly Flexible Ti3C2Tx MXene/Bacterial Cellulose Composite Films for High-Performance Electromagnetic Interference Shielding, *ACS Nano*, 2021, **15**(5), 8439–8449, DOI: 10.1021/acsnano.0c10666.

3 H. Zhao, X. Xu, D. Fan, P. Xu, F. Wang, L. Cui, X. Han and Y. Du, Anchoring Porous Carbon Nanoparticles on Carbon Nanotubes as a High-Performance Composite with a Unique Core-Sheath Structure for Electromagnetic Pollution Precaution, *J. Mater. Chem. A*, 2021, **9**(39), 22489–22500, DOI: 10.1039/D1TA06147J.

4 S. Satyamurthy, S. Savithri, R. Nirmala, A. Devarpiran and A. Ravichandran, A Case History of EMI Problems of an Optoelectronic Stabilized Sight, Proceedings of the International Conference on Electromagnetic Interference and Compatibility '99 (IEEE Cat. No. 99TH 8487), 1997, pp. 321–327, DOI: 10.1109/ICEMIC.1997.669822.

5 W. A. Radasky and M. Bäckström, Brief Historical Review and Bibliography for Intentional Electromagnetic Interference (IEMI), 2014 XXXIth URSI General Assembly and Scientific Symposium (URSI GASS), 2014, pp. 1–4, DOI: 10.1109/URSIGASS.2014.6929517.

6 K.-S. Tan and I. Hinberg, 62 - Electromagnetic Interference with Medical Devices: In Vitro Laboratory Studies and Electromagnetic Compatibility Standards. *Clinical Engineering Handbook*, ed J. F. Dyro, Biomedical Engineering, Academic Press, Burlington, 2004, pp. 254–262, DOI: 10.1016/B978-012226570-9/50068-5.

7 R. D. Leach, Failures and Anomalies Attributed to Electromagnetic Interference, InSpace Programs and Technologies Conference, 1995, pp. 1–11, DOI: 10.2514/6.1995-3654.

8 A. Ahlbom, J. Bridges, R. De Seze, L. Hillert, J. Juutilainen, M.-O. Mattsson, G. Neubauer, J. Schüz, M. Simko and K. Bromen, Possible Effects of Electromagnetic Fields (EMF) on Human Health - Opinion of the Scientific Committee on Emerging and Newly Identified Health Risks (SCENIHR), *Toxicology*, 2008, **246**(2), 248–250, DOI: 10.1016/j.tox.2008.02.004.

9 E. Kivrak, K. Yurt, A. Kaplan, I. Alkan and G. Altun, Effects of Electromagnetic Fields Exposure on the Antioxidant Defense System, *J. Microsc. Ultrastruct.*, 2017, **5**(4), 167, DOI: 10.1016/j.jmau.2017.07.003.

10 V. Lalan and S. Ganesanpotti, The Smallest Anions{,} Induced Porosity and Graphene Interfaces in C12A7:E− Electrides: A Paradigm Shift in Electromagnetic Absorbers and Shielding Materials, *J. Mater. Chem. C*, 2022, **10**(3), 969–982, DOI: 10.1039/D1TC03762E.

11 Z. Guo, P. Ren, Z. Lu, K. Hui, J. Yang, Z. Zhang, Z. Chen, Y. Jin and F. Ren, Multifunctional CoFe2O4@MXene-AgNWs/Cellulose Nanofiber Composite Films with Asymmetric Layered Architecture for High-Efficiency Electromagnetic Interference Shielding and Remarkable Thermal Management Capability, *ACS Appl. Mater. Interfaces*, 2022, **14**(36), 41468–41480, DOI: 10.1021/acsami.2c12555.

12 M. Amini, M. Kamkar, F. Rahmani, A. Ghaffarkhah, F. Ahmadijokani and M. Arjmand, Multilayer Structures of a Zn0.5Ni0.5Fe2O4-Reduced Graphene Oxide/PVDF Nanocomposite for Tunable and Highly Efficient Microwave Absorbers, *ACS Appl. Electron. Mater.*, 2021, **3**(12), 5514–5527, DOI: 10.1021/acsaelm.1c00940.

13 J. B. Anooja, K. S. Dijith, K. P. Surendran and G. Subodh, A Simple Strategy for Flexible Electromagnetic Interference Shielding: Hybrid RGO@CB-Reinforced Polydimethylsiloxane, *J. Alloys Compd.*, 2019, **807**, 151678, DOI: 10.1016/j.jallcom.2019.151678.

14 I. R. Ibrahim, K. A. Matori, I. Ismail, Z. Awang, S. N. A. Rusly, R. Nazlan, F. Mohd Idris, M. M. Muhammad Zulkimi, N. H. Abdullah, M. S. Mustaffa, F. N. Shafiee and M. Ertugrul, A Study on Microwave Absorption Properties of Carbon Black and Ni0.6Zn0.4Fe2O4 Nanocomposites by Tuning the Matching-Absorbing Layer Structures, *Sci. Rep.*, 2020, **10**(1), 1–14, DOI: 10.1038/s41598-020-60107-1.

15 Q. Qi, L. Ma, B. Zhao, S. Wang, X. Liu, Y. Lei and C. B. Park, An Effective Design Strategy for the Sandwich Structure of PVDF/GNP-Ni-CNT Composites with Remarkable Electromagnetic Interference Shielding Effectiveness, *ACS Appl. Mater. Interfaces*, 2020, **12**(32), 36568–36577, DOI: 10.1021/acsami.0c10600.

16 A. Sheng, W. Ren, Y. Yang, D. X. Yan, H. Duan, G. Zhao, Y. Liu and Z. M. Li, Multilayer WPU Conductive Composites with Controllable Electro-Magnetic Gradient for Absorption-Dominated Electromagnetic Interference Shielding, *Composites, Part A*, 2020, **129**, 105692, DOI: 10.1016/j.compositesa.2019.105692.

17 D. J. Kwon, I. J. Kwon, J. A. Milam-Guerrero, S. B. Yang, J. H. Yeum and H. H. Choi, Aramid Nanofiber-Reinforced Multilayer Electromagnetic-Interference (EMI) Shielding Composites with High Interfacial Durability, *Mater. Des.*, 2022, **215**, 110452, DOI: 10.1016/j.matdes.2022.110452.

18 D. D. L. Chung, Materials for Electromagnetic Interference Shielding, *Mater. Chem. Phys.*, 2020, **255**, 123587, DOI: 10.1016/j.matchemphys.2020.123587.

19 C. Liang, Z. Gu, Y. Zhang, Z. Ma, H. Qiu and J. Gu, Structural Design Strategies of Polymer Matrix Composites for

Electromagnetic Interference Shielding: A Review, *Nano-Micro Lett.*, 2021, **13**(1), 1–29, DOI: **10.1007/s40820-021-00707-2**.

20 L. Xu, S. Wan, Y. Heng, S. Wang, J. Yang, Y. Dong, Y. Fu and Q. Ni, Double Layered Design for Electromagnetic Interference Shielding with Ultra-Low Reflection Features: PDMS Including Carbon Fibre on Top and Graphene on Bottom, *Compos. Sci. Technol.*, 2023, **231**, 109797, DOI: **10.1016/j.compscitech.2022.109797**.

21 M. Kamkar, A. Ghaffarkhah, E. Hosseini, M. Amini, S. Ghaderi and M. Arjmand, Multilayer Polymeric Nanocomposites for Electromagnetic Interference Shielding: Fabrication{,} Mechanisms{,} and Prospects, *New J. Chem.*, 2021, **45**(46), 21488–21507, DOI: **10.1039/D1NJ04626H**.

22 J. Liu, S. Lin, K. Huang, C. Jia, Q. Wang, Z. Li, J. Song, Z. Liu, H. Wang, M. Lei and H. Wu, A Large-Area AgNW-Modified Textile with High-Performance Electromagnetic Interference Shielding, *npj Flex. Electron.*, 2020, **4**(1), 1–7, DOI: **10.1038/s41528-020-0074-0**.

23 D. T. Phan and C. W. Jung, Multilayered Salt Water with High Optical Transparency for EMI Shielding Applications, *Sci. Rep.*, 2020, **10**(1), 1–9, DOI: **10.1038/s41598-020-78717-0**.

24 S. Hu, D. Wang, Y. Kyosev, D. Kremenakova and J. Militky, The Novel Approach of EMI Shielding Simulation for Metal Coated Nonwoven Textiles with Optimized Textile Module, *Polym. Test.*, 2022, **114**(July), 107706, DOI: **10.1016/j.polymertesting.2022.107706**.

25 Z. Guo, P. Ren, B. Fu, F. Ren, Y. Jin and Z. Sun, Multi-Layered Graphene-Fe3O4/Poly (Vinylidene Fluoride) Hybrid Composite Films for High-Efficient Electromagnetic Shielding, *Polym. Test.*, 2020, **89**, 106652, DOI: **10.1016/j.polymertesting.2020.106652**.

26 V. Khade, A. B. Thirumalasetty, A. A. Rathod, Y. K. Chaoukiker and M. Wuppulluri, Flexible and Rigid Spinel Ferrite Carboneous Composite as a Future of Tunable Absorption Dominant CmWave Shielding Materials, *J. Mater. Chem. A*, 2024, **2**(15), 8914–8926, DOI: **10.1039/D3TA07624E**.

27 K. Cai, X. Han, Y. Zhao, R. Zong, F. Zeng and D. Guo, A Green Route to a Low Cost Anisotropic MoS2/Poly(Vinylidene Fluoride) Nanocomposite with Ultrahigh Electroactive Phase and Improved Electrical and Mechanical Properties, *ACS Sustainable Chem. Eng.*, 2018, **6**(4), 5043–5052, DOI: **10.1021/acssuschemeng.7b04697**.

28 C. Singh, A. Goyal and S. Singhal, Nickel-Doped Cobalt Ferrite Nanoparticles: Efficient Catalysts for the Reduction of Nitroaromatic Compounds and Photo-Oxidative Degradation of Toxic Dyes, *Nanoscale*, 2014, **6**(14), 7959–7970, DOI: **10.1039/c4nr01730g**.

29 D. Karthickraja, S. Karthi, G. A. Kumar, D. K. Sardar, G. C. Dannangoda, K. S. Martirosyan and E. K. Girija, Fabrication of Core-Shell CoFe2O4@HAp Nanoparticles: A Novel Magnetic Platform for Biomedical Applications, *New J. Chem.*, 2019, **43**(34), 13584–13593, DOI: **10.1039/c9nj02510c**.

30 P. Makuła, M. Pacia and W. Macyk, How To Correctly Determine the Band Gap Energy of Modified Semiconductor Photocatalysts Based on UV-Vis Spectra. *J. Phys*, *Chem. Lett.*, 2018, **9**(23), 6814–6817, DOI: **10.1021/acs.jpclett.8b02892**.

31 P. Saini and M. Arora, Microwave Absorption and EMI Shielding Behavior of Nanocomposites Based on Intrinsically Conducting Polymers, Graphene and Carbon Nanotubes, *New Polymers for Special Applications*, ed. A. D. S. Gomes, IntechOpen, Rijeka, 2012, DOI: **10.5772/48779**.

32 X. Li, S. Zeng, S. E, L. Liang, Z. Bai, Y. Zhou, B. Zhao and R. Zhang, Quick Heat Dissipation in Absorption-Dominated Microwave Shielding Properties of Flexible Poly(Vinylidene Fluoride)/Carbon Nanotube/Co Composite Films with Anisotropy-Shaped Co (Flowers or Chains), *ACS Appl. Mater. Interfaces*, 2018, **10**(47), 40789–40799, DOI: **10.1021/acsami.8b14733**.

33 V. Lalan, A. Puthiyedath Narayanan, K. P. Surendran and S. Ganesanpotti, Room-Temperature Ferromagnetic Sr3-YCo4O10 + δ and Carbon Black-Reinforced Polyvinylidene-fluoride Composites toward High-Performance Electromagnetic Interference Shielding, *ACS Omega*, 2019, **4**(5), 8196–8206, DOI: **10.1021/acsomega.9b00454**.

34 K. Sun, Z. Zhang, R. Fan, M. Chen, C. Cheng, Q. Hou, X. Zhang and Y. Liu, Random Copper/Yttrium Iron Garnet Composites with Tunable Negative Electromagnetic Parameters Prepared by in Situ Synthesis, *RSC Adv.*, 2015, **5**(75), 61155–61160, DOI: **10.1039/C5RA09882C**.

35 L. Sun, L. Liang, Z. Shi, H. Wang, P. Xie, D. Dastan, K. Sun and R. Fan, Optimizing Strategy for the Dielectric Performance of Topological-Structured Polymer Nanocomposites by Rationally Tailoring the Spatial Distribution of Nanofillers, *Eng. Sci.*, 2020, **12**(16), 95–105.

36 A. Rajan, K. Solaman and S. Ganesanpotti, Design and Fabrication of Layered Electromagnetic Interference Shielding Materials: A Cost-Effective Strategy for Performance Prediction and Efficiency Tuning, *ACS Appl. Mater. Interfaces*, 2023, **15**(4), 5822–5835, DOI: **10.1021/acsami.2c19016**.

37 M.-S. Cao, J.-C. Shu, X.-X. Wang, X. Wang, M. Zhang, H.-J. Yang, X.-Y. Fang and J. Yuan, Electronic Structure and Electromagnetic Properties for 2D Electromagnetic Functional Materials in Gigahertz Frequency, *Ann. Phys.*, 2019, **531**(4), 1800390, DOI: **10.1002/andp.201800390**.

38 Z. Guo, P. Ren, Z. Lu, K. Hui, J. Yang, Z. Zhang, Z. Chen, Y. Jin and F. Ren, Multifunctional CoFe(2)O(4)@MXene-AgNWs/Cellulose Nanofiber Composite Films with Asymmetric Layered Architecture for High-Efficiency Electromagnetic Interference Shielding and Remarkable Thermal Management Capability, *ACS Appl. Mater. Interfaces*, 2022, **14**(36), 41468–41480, DOI: **10.1021/acsami.2c12555**.

39 S. A. Oliver, M. L. Chen, I. Kozulin and C. Vittoria, Structure and Magnetic Properties of Barium Hexaferrite Films Deposited at Low Oxygen Pressures, *J. Magn. Magn. Mater.*, 2000, **213**(3), 326–334, DOI: **10.1016/S0304-8853(00)00004-4**.

40 M.-S. Cao, X.-X. Wang, M. Zhang, J.-C. Shu, W.-Q. Cao, H.-J. Yang, X.-Y. Fang and J. Yuan, Electromagnetic Response and Energy Conversion for Functions and Devices in Low-Dimensional Materials, *Adv. Funct. Mater.*, 2019, **29**(25), 1807398, DOI: **10.1002/adfm.201807398**.

41 Z. Wang, R. Wei and X. Liu, Fluffy and Ordered Graphene Multilayer Films with Improved Electromagnetic Interference Shielding over X-Band, *ACS Appl. Mater. Interfaces*, 2017, **9**(27), 22408–22419, DOI: **10.1021/acsami.7b04008**.

42 S.-H. Lee, D. Kang and I.-K. Oh, Multilayered Graphene-Carbon Nanotube-Iron Oxide Three-Dimensional Heterostructure for Flexible Electromagnetic Interference Shielding Film, *Carbon*, 2017, **111**, 248–257.